ChemPubSoc Europe

DOI: 10.1002/cmdc.201300134

Synergistic Inhibitor Binding to the Papain-Like Protease of Human SARS Coronavirus: Mechanistic and Inhibitor Design Implications

Hyun Lee,[a] Shuyi Cao,[a] Kirk E. Hevener,[a] Lena Truong,[a] Joseph L. Gatuz,[a] Kavankumar Patel,[a] Arun K. Ghosh,[b] and Michael E. Johnson*[a]

We previously developed two potent chemical classes that inhibit the essential papain-like protease (PLpro) of severe acute respiratory syndrome coronavirus. In this study, we applied a novel approach to identify small fragments that act synergistically with these inhibitors. A fragment library was screened in combination with four previously developed lead inhibitors by fluorescence-based enzymatic assays. Several fragment compounds synergistically enhanced the inhibitory activity of the lead inhibitors by approximately an order of magnitude. Surface plasmon resonance measurements showed that three fragments bind specifically to the PLpro enzyme. Mode of inhibition, computational solvent mapping, and molecular docking studies suggest that these fragments bind adjacent to the binding site of the lead inhibitors and further stabilize the inhibitor-bound state. We propose potential next-generation compounds based on a computational fragment-merging approach. This approach provides an alternative strategy for lead optimization for cases in which direct co-crystallization is difficult.

Introduction

Human severe acute respiratory syndrome coronavirus (SARS-CoV) was initially reported in Guangdong province, China in 2002, and quickly spread to almost 30 countries, resulting in about 8000 infections with approximately 800 deaths.[1] It was contained through public health quarantine measures after several months. The isolation of closely related strains from the horseshoe bat has been reported,[2] which suggests a potential for reemergence of the SARS-CoV by retransmission to humans from its animal reservoir. There have also been three additional human coronaviruses—HCoV-HKU1,[3] HCoV-NL63,[4] and HCoV-EMC[5]—reported since 2003. HCoV-HKU1 and HCoV-NL63 were shown to be less lethal than SARS-CoV.[3b,6] However, since April 2012, fifteen people have been infected with the most recently identified coronavirus, HCoV-EMC, nine of whom died from pneumonia and renal failure.[7] The whole genome sequence of HCoV-EMC has been characterized, and it shows close similarity to two Asian bat coronaviruses: BtCoV-HKU4 and BtCoV-HKU5.[8] This indicates a significant possibility for the emergence of new strains of SARS or new SARS-like human coronaviruses that could lead to even more deadly outbreaks.

Human SARS-CoV has a 30-kb positive RNA genome and contains two proteases: 3-chymotrypsin-like protease (3CLpro) and papain-like protease (PLpro). PLpro and 3CLpro are responsible for cleavage of the polyprotein into 16 nonstructural proteins. The first three positions between nonstructural proteins 1–4 are cleaved by PLpro, whereas the other eleven positions are cleaved by 3CLpro. Both 3CLpro and PLpro have been shown to be essential for viral replication,[9] making them attractive drug targets against SARS-CoV. 3CLpro has been intensively pursued as a drug target, and several inhibitors have been reported. They can be categorized as covalent peptidomimetic, noncovalent peptidomimetic, and nonpeptidic.[10] Unlike 3CLpro, the development of PLpro inhibitors has been very limited until recently, despite its essential role in SARS viral replication. In addition to our own work,[11] two very different types of PLpro inhibitors have been reported in recent years. First, 6-mercaptopurine (6MP) and 6-thioguanine (6TG) were identified from compound screening, with IC_{50} values of 5–20 μM.[12] Second, several natural products, diarylheptanoids isolated from *Alnus japonica*, showed inhibitory activity (IC_{50} 4.1 μM) against PLpro.[13] In addition to its primary function of viral peptide cleavage, PLpro has been recognized to be involved in deubiquitination, de-ISGylation, and viral evasion of the innate immune response.[2a,14] SARS-PLpro is a cysteine protease that contains a zinc binding motif, a catalytic triad, and a ubiquitin-like N-terminal domain (Figure 1). The sequence identity and similarity between SARS-PLpro and HCoV-EMC PLpro are 32 and 51%, respectively (Supporting Information (SI) figure S1a). Interestingly, the predicted structure of HCoV-

[a] Dr. H. Lee, S. Cao, Prof. K. E. Hevener, L. Truong, J. L. Gatuz, K. Patel, Prof. M. E. Johnson
Center for Pharmaceutical Biotechnology and
Department of Medicinal Chemistry & Pharmacognosy
University of Illinois at Chicago, Chicago, IL 60607 (USA)
E-mail: mjohnson@uic.edu

[b] Prof. A. K. Ghosh
Departments of Chemistry and Medicinal Chemistry
Purdue University, 560 Oval Drive, West Lafayette, IN 47907 (USA)

Supporting information for this article is available on the WWW under http://dx.doi.org/10.1002/cmdc.201300134.

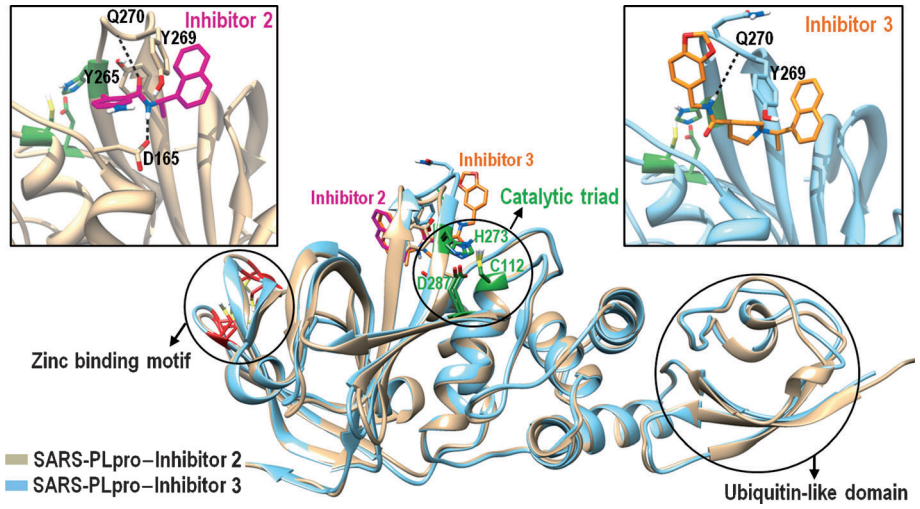

Figure 1. Overlay of the two known PLpro co-crystal structures. The inhibitor **2** bound (PDB ID: 3E9S) structure is shown in tan, and the inhibitor **3** bound (PDB ID: 3MJ5) structure is shown in cyan. The PLpro enzyme contains an intact zinc binding motif (left), a catalytic triad (middle), and a ubiquitin-like N-terminal domain. Inhibitor **2** and **3** interactions with the PLpro enzyme are shown in the expanded square boxes in detail.

EMC PLpro is very similar to that of SARS-PLpro (SI figure S1 b). The three catalytic residues (C112, H273, and D287) and four cysteines in the zinc binding motif are identical in these two PLpro enzymes. In addition, nine highly conserved residues in many other PLpro enzymes are also observed in HCoV-EMC PLpro (highlighted in yellow in SI figure S1 a). This suggests that HCoV-EMC PLpro may possess characteristics similar to that of SARS-PLpro.

By using high-throughput screening (HTS) and structure-based drug design, we previously developed a series of noncovalent PLpro inhibitors that show promise as potential therapeutic agents.[11] Inhibitor **1** (GRL-0068S) has shown an inhibitory activity (IC_{50} value) of 0.29 μM and antiviral activity (EC_{50}) of 5.2 μM (see Table 1 below for inhibitor structures). Inhibitors **2** (GRL-0617S), **3** (GRL-0667S), and **4** (GRL-0737S) have exhibited inhibitory activities of 1.32, 0.64, and 1.36 μM, with antiviral activities of 15, 9.1, and 9.1 μM, respectively.[11a,15] These inhibitors represent two active chemical scaffolds, with **1** and **2** representing the first (scaffold **A**), and **3** and **4** representing the second (scaffold **B**). Because these four lead inhibitors show moderate antiviral activity against SARS-CoV, their potencies must be further improved before development into clinical candidates. Analysis of the two available PLpro structures with inhibitors **2** and **3** and subsequent molecular modeling studies revealed that these leading inhibitors bind to a pocket formed mostly by the G267–G272 loop and the Leu163 side chain, distinct from the catalytic site shown in green in Figure 1.[11b,15] The inhibitors appear to block substrate access to the entrance of the catalytic site of the PLpro enzyme. Both scaffolds bind to a similar area, although scaffold **A** (inhibitors **1** and **2**) blocks only a little over half of the area blocked by scaffold **B** (inhibitors **3** and **4**).

One way to improve the potency of these lead inhibitors would be to optimize the compounds by expanding into unoccupied space near their current binding site. This would require the synthesis of larger compounds, a process that consumes significant amounts of time and resources, and may or may not result in better binding affinity and potency. An alternative strategy is the application of fragment-based drug design (FBDD) methodology, which has become a well-established method for lead optimization.[16] In many cases, FBDD has been used to discover small scaffolds for further optimization or to find two small fragments that can be linked together to produce a more potent inhibitor.[16e] To be able to link two small fragments, it is typically necessary to solve crystal structures with each fragment. In many cases, obtaining this structural information can be very challenging and time-consuming due to the typical weak binding affinity of fragments for their target enzymes. In this study, we used FBDD in combination with detailed enzymatic analysis as a means to further optimize our leading inhibitors without the use of crystallography. By testing a small library of fragment compounds in the presence of each of the lead inhibitors, we were able to identify fragments that synergistically improve the potency of the leading inhibitors. Additional enzymatic analyses (including mechanism of inhibition and mutual exclusivity studies, described in detail below) and computational studies were used to predict the fragment binding locations. Finally, a fragment-merging strategy was employed to predict next-generation compounds that are able to recapitulate the binding position of the lead inhibitors as well as key binding features of the identified fragments.

Results and Discussion

Fragment library screening

The two currently developed SARS-CoV PLpro inhibitor scaffolds do not bind at the catalytic site of the PLpro protease, but at a separate nearby binding site cradled between the L163 residue and binding loop 2 (G267–G272). This leaves the catalytic site unoccupied during inhibition. Although the catalytic pocket is small, there is a reasonable probability that fragment compounds could successfully bind to this location and enhance inhibitory activity of the lead inhibitors. The Zenobia library, consisting of 352 chemically and structurally diverse fragment-like compounds, was experimentally screened in the presence of each of the four previously discovered lead inhibitors. All fragment compounds were tested by continuous kinetic enzymatic assays as described in the Experimental Section below. A replicate plot of inhibitor **2** with the 352 fragments showed highly reproducible results (SI figure S2 a). The

replicate plots of the other lead inhibitors were similar to that of inhibitor **2**. Of the 352 fragment-like compounds, 17, 14, 16, and 16 fragments showed >30% increase in enzyme inhibition when tested at a fragment concentration of 200 μM in the presence of inhibitors **1**, **2**, **3**, and **4**, respectively. Percentage efficiency indices (PEI) for all 352 fragments were calculated as a hit selection criteria according to the method of Abad-Zapatero et al.; percent inhibition was divided by the molecular weight (M_r) of each compound.[17] Compounds with PEI values of 1.5 or greater were classified as hits, and the medium-range compounds (PEI 2.0–4.0) were selected for further testing. High PEI-range compounds (>4.0) were classified as outliers due to the strong likelihood of nonspecificity. The histogram of PEI values for all 352 fragments in combination with each of our four lead inhibitors is shown in SI figure S2b. A total of 13 fragments were in the medium PEI range and were selected for further studies.

The IC_{50} values of the 13 selected fragments in the absence of any lead inhibitors were first determined. The IC_{50} values varied from 149 μM (fragment **F2**) to 427 μM (fragment **F6**), and are summarized in Table 1. Next, the IC_{50} values of the four lead inhibitors were determined in the presence of each of the 13 fragment-like compounds. Of the 13 fragment-like compounds, eight fragments showed synergistic enhancement, with IC_{50} value decreases of more than threefold for at least one of the lead inhibitors. The IC_{50} values of inhibitor **1** were enhanced 9.1- and 8.1-fold by fragments **F4** and **F8**, respectively, relative to that of each lead inhibitor alone (Table 1). Fragment **F7** showed the strongest synergy with inhibitor **2**, enhancing its IC_{50} value by 3.9-fold, and two other fragments (**F4** and **F8**) also equally enhanced inhibitor **2** by 3.1-fold. The IC_{50} values of inhibitors **3** and **4** were enhanced 11.6- and 8.5-fold, respectively, by fragment **F3**, while the same compound, **F3**, did not improve the IC_{50} value of inhibitor **2**. Fragment **F3** appeared to have better synergy with scaffold **B** inhibitors than with those representing scaffold **A**. Fragments **F8** and **F6** also showed significant synergistic activity with inhibitors **3** and **4**, respectively.

Six of the eight fragments exhibited reversible enzyme recovery, whereas two—**F3** and **F5**—showed respective recovery rates of only 25 and 31%. PLpro is a cysteine protease that contains a cysteine in the active site, and these partially irrever-

Table 1. IC_{50} value comparison of four lead inhibitors in combination with fragment compounds from the Zenobia library.

	Lead Inhibitor IC_{50} [μM]							
	1 (GRL-0068S)		**2** (GRL-0617S)		**3** (GRL-0667S)		**4** (GRL-0737S)	
	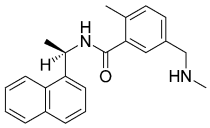		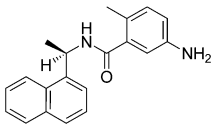		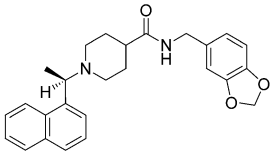		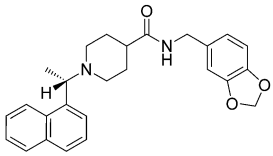	
	0.29 ± 0.07		1.32 ± 0.08		0.64 ± 0.06		1.36 ± 0.08	
Fragment IC_{50} [μM]	**1** + Frag.	FD[a]	**2** + Frag.	FD[a]	**3** + Frag.	FD[a]	**4** + Frag.	FD[a]
F1 (ZT0009) 188 ± 36	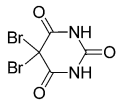							
	0.23 ± 0.04	1.3	2.94 ± 0.09	0.45	0.20 ± 0.04	3.2	0.79 ± 0.19	1.7
F2 (ZT0273) 149 ± 15	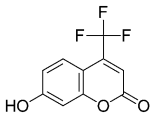							
	0.056 ± 0.012	5.2	0.66 ± 0.01	2.0	0.18 ± 0.01	3.6	0.49 ± 0.06	2.8
F3 (ZT0408) 392 ± 28	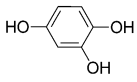							
	0.049 ± 0.021	5.9	2.68 ± 0.52	0.49	0.055 ± 0.027	11.6	0.16 ± 0.03	8.5
F4 (ZT0426) 212 ± 27	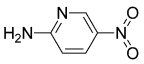							
	0.032 ± 0.013	9.1	0.42 ± 0.09	3.1	0.13 ± 0.03	4.9	0.25 ± 0.04	5.4
F5 (ZT0470) 388 ± 10	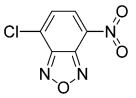							
	0.050 ± 0.011	5.8	1.25 ± 0.01	1.1	0.17 ± 0.04	3.8	0.44 ± 0.08	3.1
F6 (ZT0537) 427 ± 20	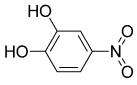							
	0.051 ± 0.005	5.7	0.53 ± 0.06	2.5	0.088 ± 0.018	7.3	0.21 ± 0.05	6.5
F7 (ZT0626) 292 ± 6	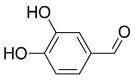							
	0.048 ± 0.005	6.0	0.34 ± 0.13	3.9	0.12 ± 0.01	5.3	0.26 ± 0.03	5.2
F8 (ZT0834) 279 ± 38	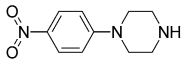							
	0.036 ± 0.013	8.1	0.43 ± 0.08	3.1	0.074 ± 0.019	8.7	0.37 ± 0.11	3.7

[a] Fold decrease in IC_{50} value.

sible fragments may covalently interact with this residue. Covalently interacting compounds are likely to be nonspecifically reactive and usually have toxicity issues. Therefore, fragment **F3** may not be a good candidate, although it was the best enhancer for scaffold **B** inhibitors (inhibitors **3** and **4**). Similarly, these results indicate that fragment **F5** may also exhibit problems with irreversibility. Two ligand-efficiency-related indices, binding efficiency index (BEI) and surface binding efficiency index (SEI), were calculated as described.[18] BEI relates potency to the molecular weight of each compound, while SEI is an index that monitors the potency gains as polar surface area (PSA) increases. BEI and SEI for these eight fragments and four lead inhibitors were calculated by simple equations: pIC_{50} divided by M_r for BEI and pIC_{50} divided by PSA for SEI.[17] The PSA value is an important indicator related to oral bioavailability and intestinal permeability.[19] The BEI values of fragments **F3**, **F4**, and **F7** were >25, suggesting that they are outliers due to the possibility of nonspecific interaction (SI figure S2c). Fragment **F7** contains an aldehyde, which is likely to exhibit nonspecific affinity for the cysteine residue in the catalytic site of the PLpro enzyme. Thus, considering both ligand efficiency indices and enzyme activity recovery rate, fragments **F8**, **F8**, **F6**/**F8**, and **F6** are the best enhancers for inhibitors **1**, **2**, **3**, and **4**, respectively.

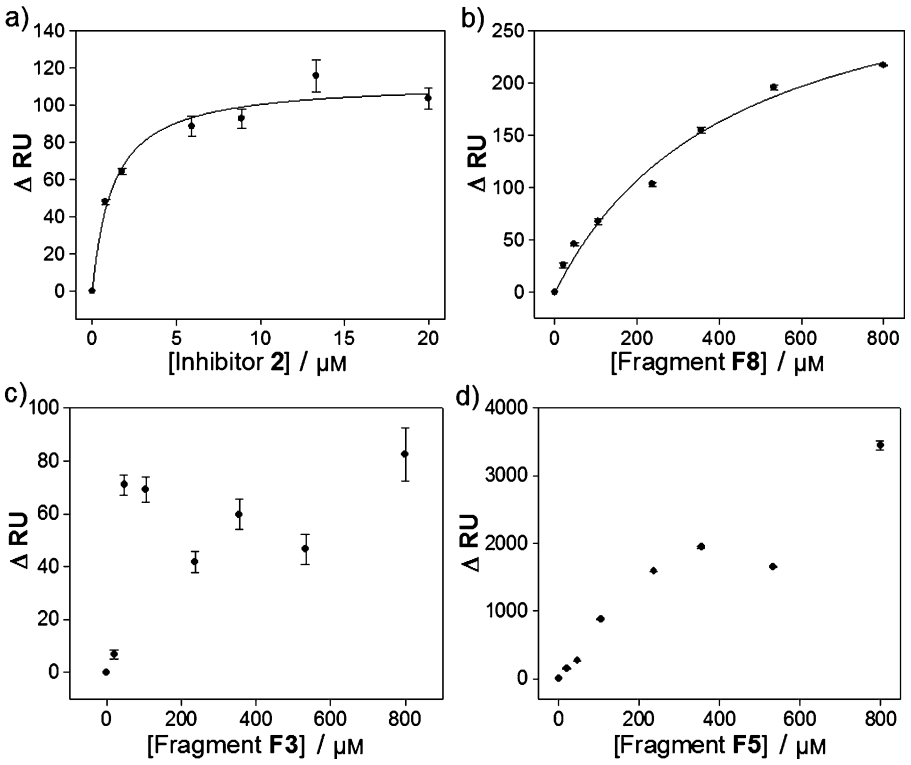

Figure 2. Dissociation equilibrium constant (K_D) determination by SPR binding analysis: fitting curves of a) inhibitor **2** and b) fragment **F8**. The response unit difference (ΔRU) plots of c) fragments **F3** and d) **F5** with respect to concentration of each compound are shown, and suggest random and nonspecific binding, respectively. Data in panels a) and b) were fit to a single rectangular hyperbolic curve to calculate K_D (see Experimental Section for details).

Table 2. Dissociation equilibrium constants (K_D determined by SPR) and mechanism of inhibition.

Compound	K_D [μM]	Inhib. Type	K_i [μM]
1 (GRL-0068S)	1.69 ± 0.27	noncompetitive ($\alpha = 2.6$)	0.42
2 (GRL-0617S)	1.04 ± 0.16	noncompetitive ($\alpha = 2.0$)	2.00
3 (GRL-0667S)	0.97 ± 0.03	noncompetitive ($\alpha = 2.7$)	0.42
4 (GRL-0737S)	1.06 ± 0.09	noncompetitive ($\alpha = 2.5$)	0.80
F2 (ZT0273)	202 ± 89	noncompetitive ($\alpha = 1.0$)	207
F6 (ZT0537)	461 ± 30	noncompetitive ($\alpha = 1.5$)	234
F8 (ZT0834)	437 ± 36	noncompetitive ($\alpha = 1.6$)	242

Binding analysis by SPR

Although we observed IC_{50} value enhancement by the fragments through dose–response curves using enzymatic assays, it is possible that the results could be due to nonspecific interactions between the PLpro enzyme and the fragments. Enzyme assays alone can lead to false positives in some cases. To investigate this further, orthogonal binding analyses by surface plasmon resonance (SPR) were performed, and the dissociation equilibrium constants (K_D), which reflect binding affinity, were determined for each of the four lead inhibitors **1**–**4** and the seven newly identified fragments **F2**–**F8**. Fragment **F1** was excluded from these studies due to its low IC_{50} enhancement. The binding affinities of inhibitors **1**–**4** varied between 0.97 and 1.67 μM as determined by SPR, which were in a range similar to their IC_{50} values (Table 2 and Figure 2a). Promisingly, the binding affinities of fragments **F2**, **F6**, and **F8** were respectively 202, 461, and 437 μM. The K_D fitting curve of **F8** is shown in Figure 2b as an example. However, three fragments, **F3**, **F4**, and **F7**, were suspected of forming nonspecific interactions due to their unusually high BEI values as noted above. SPR analyses confirmed that these three fragments, as well as fragment **F5**, all bind nonspecifically. Fragments **F3**, **F4**, and **F7** did not show a typical dose–response curve as their concentrations increased; instead, they showed a random binding pattern as shown Figure 2c for **F3**. Fragment **F5** did show a typical dose–response curve, but SPR response units increased to nearly 4000 RU when its concentration increased to 800 μM (Figure 2d). This is likely due to multisite binding caused by aggregation rather than one-to-one interaction with the PLpro enzyme, suggesting that the fragment may bind to many different locations on the PLpro enzyme.

Mechanism of inhibition studies

Mechanism of inhibition studies have not been thoroughly described for the lead inhibitors. Prior studies suggested that inhibitors **2** and **3** behave as competitive inhibitors.[14–15] Two crystal structures with these compounds verify that they bind at the entrance of the catalytic site, blocking substrate access to the site. Although these lead inhibitors do not bind directly to the catalytic site, they nonetheless display competitive inhibition patterns. To thoroughly investigate the inhibition mechanism of both lead inhibitors and fragment compounds, kinetic studies for each compound were performed with the enzyme–inhibitor complexes and varying substrate concentrations. The data were fitted to four equations [Eqs. (2)–(5) in Experimental Section] and three plots (Michaelis–Menten, Lineweaver–Burk, and Dixon), each using SigmaPlot Enzyme kinetics Module 1.3. Akaike information criterion-corrected (AICc) values were used to determine the best fit equation,[20] for which the lowest AICc value corresponds to the best fit equation. To determine which equation fits best, the AICc value difference must be at least two units from the next lowest.[20] All four previously developed lead inhibitors showed noncompetitive inhibition with unequal binding affinity to free enzyme (E) and substrate-bound enzyme (ES), where the alpha (α) value is not equal to 1 (Table 2). All four lead inhibitors showed α values greater than 1, which indicates the binding affinity to free enzyme is tighter than that of ES. Dixon plots for noncompetitive inhibition of inhibitor **1** ($\alpha = 2.6$) with respect to the substrate are shown in Figure 3a, and the resulting K_i value was 0.42 μM. All three fragments showed noncompetitive inhibition with different α values as well. Fragments **F6** and **F8** had α values greater than 1 ($\alpha > 1$), indicating that these fragments also behave similarly to the lead inhibitors, although α values of these fragments were smaller than those of the lead inhibitors. This may explain why **F8** displayed the strongest effect with the three lead inhibitors (**1**, **2**, and **3**), whereas fragment **F6** exhibited the strongest synergistic effect with scaffold **B** inhibitors (**3** and **4**). Dixon plots for noncompetitive inhibition of fragment **F8** ($\alpha = 1.6$) are shown in Figure 3b, and the K_i value was determined to be 242 μM. Because all four lead inhibitors and two fragments showed noncompetitive inhibition with $\alpha > 1$, it is likely that these compounds bind to another site that is not a catalytic site, hindering substrate binding to the enzyme. Therefore, these studies suggest that it is unlikely that these newly identified fragment-like compounds bind to the catalytic site of the PLpro enzyme.

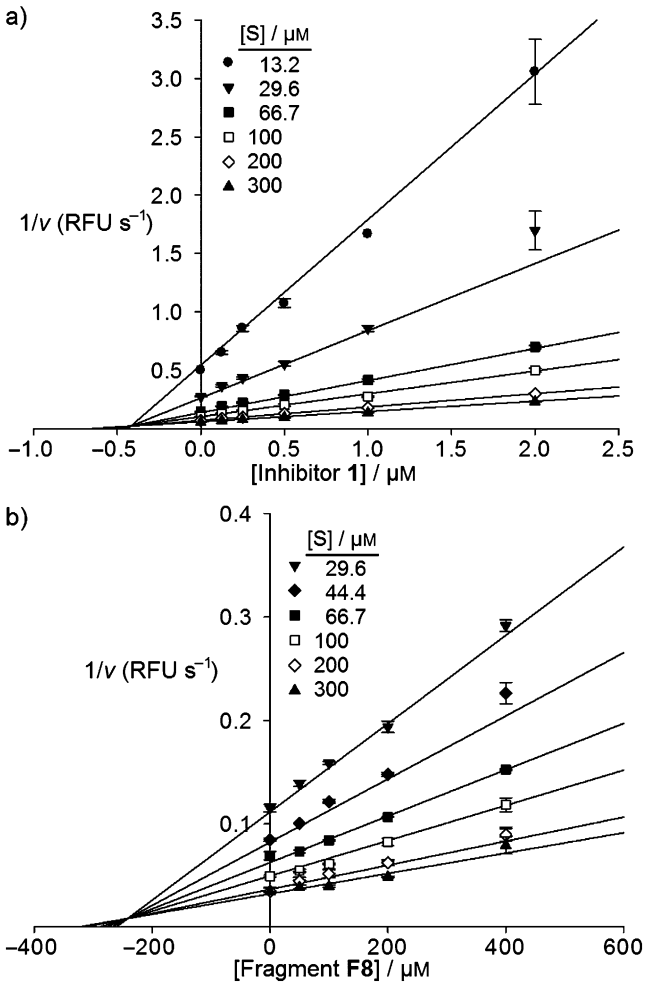

Figure 3. Inhibition mode of lead inhibitors and fragments: Dixon plots for noncompetitive inhibition of a) inhibitor **1** (GRL-0068) and b) fragment **F8** with respect to the substrate Z-Arg-Leu-Arg-Gly-Gly-AMC at indicated concentrations. K_i values determined for inhibitor **1** and fragment **F8** were 0.42 and 241 μM, respectively. Equations (2)–(5) (see the Experimental Section section) in the SigmaPlot Enzyme Kinetics Module 1.3 were used to fit the experimental data. The noncompetitive inhibition model was the best fit for both inhibitor **1** and fragment **F8**, producing respective α values of 2.6 and 1.6.

Computational solvent mapping

From our mechanism of inhibition and binding synergy/mutual exclusivity analyses, we determined that the newly identified fragment-like compounds bind to a site separate from that of the lead inhibitors. Unfortunately this information is insufficient to identify where the fragments bind on the PLpro enzyme. Therefore, we investigated all possible binding site candidates. The unexplored catalytic pocket was designated as candidate fragment binding site 1, although our mechanism of inhibition studies indicated that this location was not likely to be the fragment binding site. To identify additional candidate fragment binding sites, we performed a series of computational solvent mapping experiments, or "hot spot" analyses, using the FTMAP server (see Experimental Section).[21] FTMAP is a multistage protein mapping algorithm that is based on a fast Fourier transform (FFT) correlation. This approach can efficiently search for potential binding sites on the entire surface of the protein. Two model systems, crystal structures of inhibitor **2** bound to PLpro (PDB ID: 3E9S) and inhibitor **3** bound to PLpro (PDB ID: 3MJ5), were used for the analyses. These two provided representative crystal structures for each compound scaffold. Using 50 ns molecular dynamics (MD) simulations for each system (3E9S, 3MJ5), we determined that the major fluctuations of both structures come from the zinc binding motif and a β sheet forming the catalytic triad. Representative snapshot structures were extracted from the

simulations as discussed below (see Experimental Section) and submitted to the FTMAP server, which performed a fragment-based binding site analysis. Two strong candidate fragment binding sites were identified by analyzing the original structures and consensus clusters of the probe molecules used (see Experimental Section below). The two hot spots identified by this analysis included an extension of the original binding site of the lead inhibitors and one cavity in the palm region (shown in Figure 4a). Hot spot 1 was larger than the lead inhibitor binding site and included an additional cavity unoccupied by the lead inhibitors. This binding site has been previously discussed as a possible substrate recognition site.[11] This extended cavity is composed of five residues: R167, E168, M209, D303, and T302. The second position identified by FTMAP, hot spot 2, was located >10 Å away from both the lead inhibitor binding site and the catalytic site of PLpro. It is encompassed by the zinc binding motif and the palm region. Lastly, the small volume containing the catalytic triad (site 1) was not identified by FTMAP, likely due to the smaller size of this pocket.

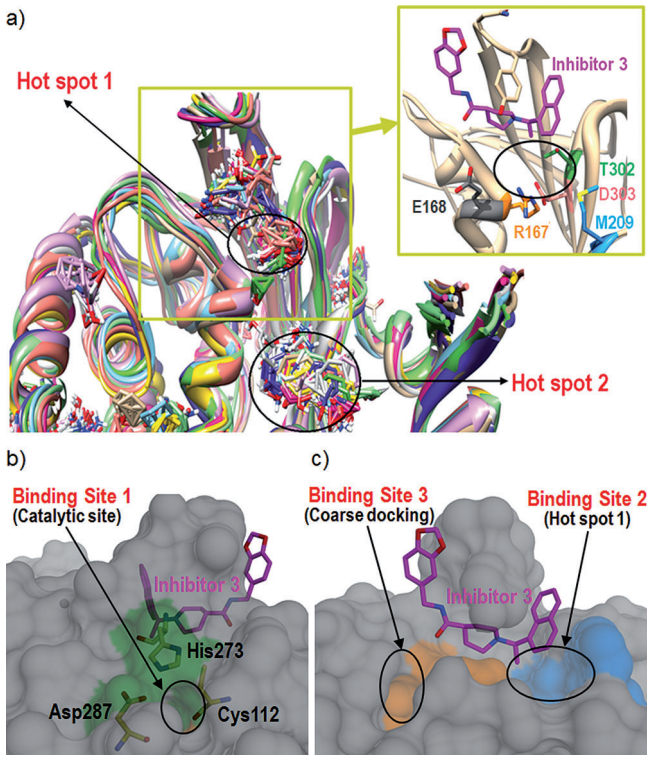

Figure 4. Fragment binding site analysis results from FTMAP and identification of potential binding sites: a) Shown are two potential binding sites identified by FTMAP using the co-crystal structure of PLpro with inhibitor **3**. The first candidate site (upper circle) is an extension of the lead inhibitor's binding site, formed by E186 (grey), R187 (orange), M209 (blue), T302 (green), and D303 (pink). The second candidate site (lower circle) is encompassed by the zinc binding motif and the palm region. b) Unoccupied catalytic pocket surrounded by three residues (C112, H273, and D287). This small pocket was initially considered a potential fragment binding site 1, but subsequently eliminated. c) Two small unoccupied pockets near the PLpro lead inhibitor binding site. Binding site 2 was identified by FTMAP hot spot analysis, and the third putative binding site (binding site 3) was identified by docking studies in the region near the lead inhibitor binding site. The image in panel c) was prepared by 90° counterclockwise rotation of the image in panel b), which gives a better view of binding site 2.

Fragment binding site analysis

Structural analysis and computational studies identified four potential fragment binding sites, three of which are located within 10 Å of the binding sites of the lead inhibitors. Candidate binding site 1, shown in green, is the unoccupied catalytic pocket (Figure 4b), identified by analysis of the co-crystal structures available. Candidate binding site 2 was identified by FTMAP using computational solvent mapping, as discussed above and in the Experimental Section. The surrounding residues of candidate binding site 2, located to the right of the lead inhibitor binding site in Figure 4c, are shown in blue. Additional coarse docking studies with hit fragment compounds (see Experimental Section) identified another shallow binding site (designated candidate binding site 3, shown in orange in Figure 4c). The mechanism of inhibition analyses and mutual exclusivity studies discussed above indicated that the fragments bind in combination with the lead inhibitors in a distinct and separate binding site of the enzyme. This important observation lays the foundation for future fragment–inhibitor merging or linking studies proposed below.

To further investigate the candidate fragment binding sites and to predict the most likely binding conformation of the fragments within each site, we performed a series of computational binding free energy calculations. These studies, described in detail in the Experimental Section, used a combination of molecular docking, molecular simulations, and molecular mechanics/Poisson–Boltzmann surface area (MM/PBSA) calculations to predict the binding free energy (ΔG_{bind}) of the lead inhibitors when the synergistic fragments were placed in the adjacent candidate binding sites. These studies were performed using three potential binding sites: site 1 (the catalytic site), site 2 (the extended lead inhibitor binding site), and site 3 identified by coarse docking. Hot spot 2 was excluded from these studies due to the large distance (>10 Å) from the inhibitor binding site. Hot spot 2 is very shallow, highly solvent-exposed, and located between the zinc binding motif and the palm region (see Figure 4a). More importantly, it appears likely that even if binding of small fragments to this position could cause some degree of conformational changes to these two regions, any structural change would not be likely to affect the lead inhibitor binding site to enhance their IC_{50} values to the extent observed. For these reasons, as well as the impracticality of fragment linking or merging strategies at such a distance, hot spot 2 was excluded from further analyses.

The calculated free energies of binding of the lead inhibitors, with a fragment placed in each successive candidate site, were then compared with the experimentally determined binding affinity (IC_{50}) of the lead inhibitors with the synergistic fragments to predict the most likely fragment binding site. For the purposes of these studies, the binding conformations of inhibitors **2** and **3** from the co-crystal structures, representing scaffolds **A** and **B**, were used. Fragment **F8** was selected for use in these studies due to its strong synergistic effect on both inhib-

itors **2** and **3**. The fragment was docked into each of the three candidate binding sites discussed above, and three docking poses for each fragment were selected for further simulation (see Experimental Section). Post-analysis of the simulation results by MM/PBSA allowed calculation of the binding free energies of the lead inhibitors for each simulation, as shown in Figure 5.

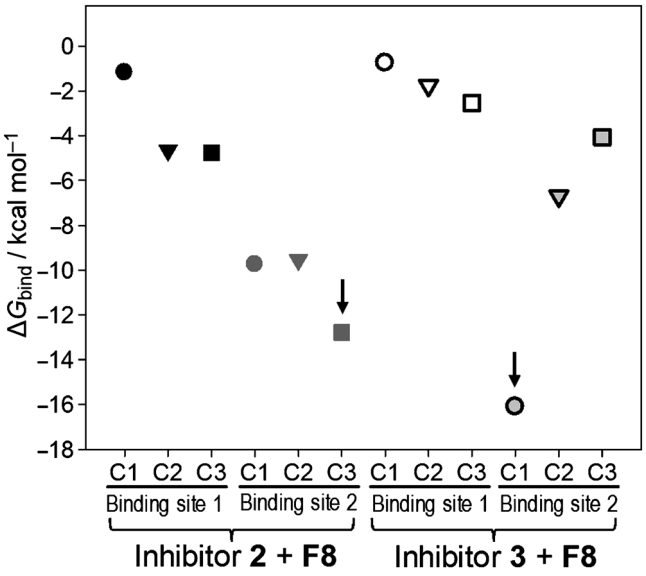

Figure 5. Calculated binding free energies of inhibitors **2** and **3** when fragment **F8** is docked into various candidate sites. Three different docked conformations, C1 (circles), C2 (triangles), and C3 (squares) at each binding site were selected for calculations. More negative numbers represent better binding conformation, with those marked by black arrows being the best.

We initially noted that fragment **F8** was not stable in binding site 3, and repeatedly drifted from the site by the 20 ns mark, regardless of its starting position. This suggests that the shallow and solvent-exposed binding site 3 is also not an appropriate position for fragment binding. Hence, the site was also removed from consideration, and further analysis of this site was not performed. Additionally, an analysis of the MM/PBSA results (Figure 5, SI tables S1 and S2) revealed that the catalytic site, site 1, was also not a favorable position for fragment binding. The binding free energy values for the inhibitor with fragment **F8** at this position were higher than those calculated for the inhibitor alone as well as the experimentally derived results. These results, taken together with the experimental results discussed above, indicate that the catalytic site is most likely not the binding site of the identified synergistic fragments. Favorable results that closely aligned with experimental values were obtained, however, when the fragments were placed at binding site 2 (shown in Figure 6), consistent with synergistic activity. We noted a preference for a positive charge, as observed in the **F8** piperazine amine group, to be placed into an anionic pocket of site 2, defined by D303, T302, Y274, and D165, which, in combination with the established binding features of the lead inhibitors, resulted in a clear gain in their calculated binding affinity. An additional edge-to-face

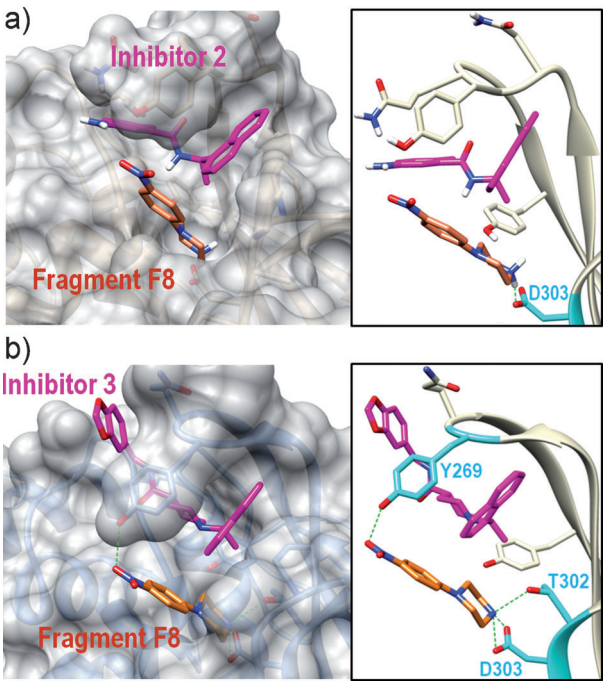

Figure 6. The most probable binding conformation of fragment **F8** (orange) in combination with lead inhibitors a) **2** (magenta) and b) **3** (magenta). Residues of the PLpro enzyme that interact with fragment **F8** are shown in the boxes at right, with hydrogen bonds shown in green.

π stacking interaction between the naphthalene ring system and the aromatic ring system of fragment **F8** (visible in Figure 6) may further stabilize the lead inhibitors in their binding conformations.

To prioritize compound candidates for future synthesis and testing, we undertook a series of fragment-merging and docking analyses, using the information determined from the binding site prediction studies discussed above. Our fragment-merging strategy involved the elimination of a potentially problematic nitroaromatic ring of fragment **F8** and the direct incorporation of the piperazine ring into the lead inhibitor scaffold, as shown in Figure 7. A series of proposed compounds were designed using a variety of linking groups and positions (discussed in the Experimental Section below), and docked into the extended binding site defined by the lead inhibitor and binding site 2 (Table 3). Proposed compounds were selected by score and their ability to successfully recapitulate the key binding features of the inhibitor and synergistic fragment, including the lipophilic interactions of the naphthalene ring system and the positioning of the positively charged amine of the piperazine into the key anionic pocket discussed above.

Conclusions

In attempts to improve the potency of currently developed leading PLpro inhibitors, a fragment-like library was enzymatically tested in combination with four lead inhibitors. We discovered a total of eight fragment-like compounds that synergistically enhanced the inhibitory activity of lead inhibitors. An

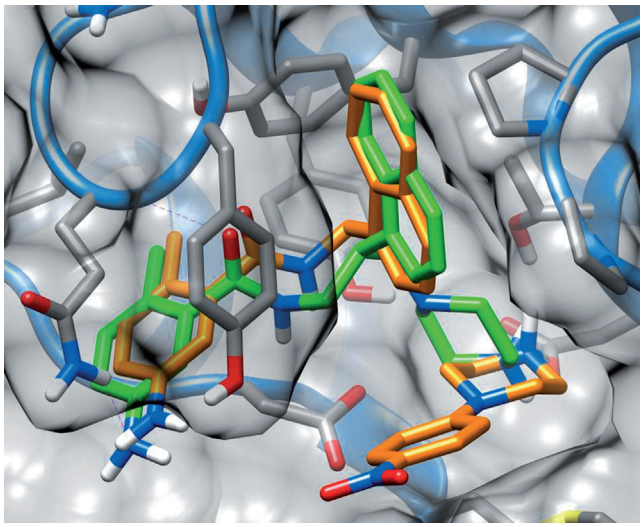

Figure 7. One of the compounds proposed for synthesis and testing by the fragment-merging strategy: The proposed compound **M1** (green carbon atoms), after molecular docking, is able to recapitulate the crystallographic position of the inhibitor and the predicted position of the synergistic fragment (orange carbons). The potentially problematic nitroaromatic ring of the fragment is removed in favor of the merged compound, which directly incorporates the piperazine ring into the lead inhibitor scaffold. Key binding features of the inhibitor and synergistic fragment are conserved, including the lipophilic interactions of the naphthalene ring system and the positioning of the positively charged amine of the piperazine into a key anionic pocket.

Table 3. Compounds proposed for synthesis and testing by fragment merging and docking calculations.

Compd	GRL-0617S + ZT0834 Structure[a]	Docking Score
M1	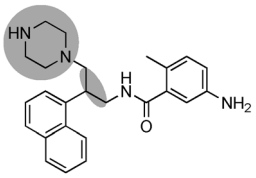	−7.837
M2	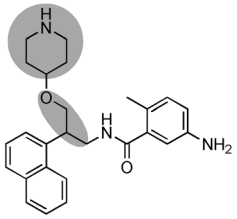	−6.421
M3	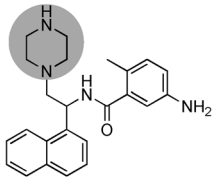	−5.735

[a] Structure portions not highlighted are from the lead inhibitors, and moieties highlighted in grey circles came from fragment **F8**. Linkers between the lead inhibitor and a fragment part are highlighted with a small grey oval.

orthogonal binding analysis by SPR confirmed the binding of three of these fragments and also determined their direct binding affinities (K_D). Our characterization assays of the binding mechanism of the two newly identified fragment compounds showed noncompetitive inhibition. This indicated that the synergistic fragment compounds did not bind to the catalytic site of the PLpro enzyme. Computational analysis predicted several potential fragment binding sites, and more expansive studies revealed a preference for fragment binding to site 2, an extension of the lead inhibitor binding site, when the inhibitor binding site was occupied by representative structures. Enzymatic characterization and computational studies suggest that these fragments, by binding adjacent to the binding site of the lead inhibitors, are able to further stabilize the inhibitor-bound state. Using the structural information revealed by these studies, we were able to apply a fragment-merging strategy to suggest several next-generation compounds with high predicted binding affinity. The novel approach described herein may be beneficial for other cases in which direct crystallization studies prove difficult.

Experimental Section

Reagents and chemicals: The Zenobia library, consisting of 352 structurally diverse small fragment-like compounds, was purchased from Zenobia Therapeutics. The molecular weights of these 352 compounds vary between 94.12 and 285.9 Da, with a mean molecular weight of 154 Da. The mean number of hydrogen bond donors and acceptors are 1.4 and 2.6, respectively. The mean clog*P* and topological polar surface area (tPSA) values are 1.6 and 52 Å^2, respectively. The solubility of each compound was verified by the vendor to be at least 200 mM in 100% DMSO. The 352 compounds in the Zenobia library are functionally and chemically diverse and synthetically accessible for further optimization. They are categorized and distributed as shape-diverse mixtures of eight compounds in 96-well plate columns. The four lead inhibitors **1**–**4** were provided by Dr. A. K. Ghosh. The PLpro substrate, Z-Arg-Leu-Arg-Gly-Gly-AMC, was purchased from Bachem Bioscience.

Tested compounds: Previously developed inhibitors **1**–**4** were synthesized by Dr. A. K. Ghosh, and the purity of each compound was confirmed by NMR as described.[12,13] Fragments **F1**–**F8** were repurchased from Sigma. Compound purity was determined by NMR to be $\geq$95%. NMR spectra for each fragment compound listed in Table 1 are included in the Supporting Information.

Cloning, expression, and purification of SARS-CoV PLpro: The PLpro gene (SARS-CoV polyprotein residues 1541–1855) with human rhinovirus 3C protease cleavage site and His tag (LEVLFQGPHHHHHH) at the C terminus was initially prepared by codon-optimized gene synthesis (BioBasic Inc.) and cloned into a pET15b vector between NcoI and XhoI sites. A stop codon was added immediately after the last PLpro gene to generate native PLpro without any tag. Rosetta2(DE3) cells (Novagen) containing the recombinant plasmid were grown to an OD_{600} of 0.6 at 37 °C by shaking at 200 rpm in LB medium (2 L volume) containing ampicillin (100 μg mL^{-1}) and chloramphenicol (34 μg mL^{-1}). Native PLpro was expressed by adding 0.5 mM IPTG with incubation continued at 25 °C for 4 h. The cells were then harvested by centrifugation at 8000 rpm (Beckman JA-10) for 15 min and resuspended in lysis buffer (1 mg mL^{-1} lysozyme and protease inhibitor cocktail in buffer A: 20 mM Tris·HCl (pH 7.5), 10 mM β-mercaptoethanol

(BME)) and were sonicated on ice. The lysate was centrifuged at 19000 rpm (Beckman JA-20) for 30 min, and the supernatant was collected. The supernatant was then subjected to a 40% ammonium sulfate fractionation. The suspension was centrifuged at 19000 rpm (Beckman JA-20) for 20 min, and the resulting pellet was resuspended in buffer B (1.5 M ammonium sulfate, 20 mM Tris, pH 7.5, 10 mM BME) and centrifuged at 19000 rpm (Beckman JA-20) for 20 min to remove precipitate. The supernatant was loaded onto a 5 mL phenyl-Sepharose 6 Fast-Flow HS column (Amersham BioSciences, Piscataway, NJ, USA) equilibrated with buffer B. The protein was eluted with a stepwise gradient of 20, 40, 60, and 100% buffer A. The native PLpro eluted at 100% buffer A. Fractions containing PLpro were pooled and dialyzed with buffer A overnight at 4 °C and loaded onto a HiTrap QXL (Amersham BioSciences). The protein was eluted with a stepwise gradient with buffer C (20 mM Tris, pH 7.5, 0.5 M NaCl, 10 mM BME), and PLpro eluted out at ~20% buffer C. Pure SARS-CoV PLpro fractions were combined, buffer-exchanged into buffer A containing 20% glycerol, and stored at −80 °C. Purity was >90%, as determined by SDS-PAGE analysis.

Compound screening: The Zenobia library was purchased as 200 mM DMSO stocks. All 352 compounds were experimentally tested against PLpro in combination with the four previously developed PLpro inhibitors. PLpro activity was measured by a continuous kinetic assay with ubiquitin-derived substrate Z-Arg-Leu-Arg-Gly-Gly-AMC (Bachem Bioscience) that generates a fluorescence signal (excitation λ: 360 nm; emission λ: 450 nm) when aminomethylcoumarin (AMC) is cleaved. For primary screening, Zenobia compounds were first diluted to 10 mM DMSO stock in a 384-well plate (Corning Inc.) from 200 mM original compound solutions. Assay buffer (7.5 μL) containing 50 mM HEPES, pH 7.5, 0.01% Triton X-100, 0.1 mg mL^{-1} BSA, and 2 mM GSH was distributed to black low-volume 384-well plates (Corning Inc.). Zenobia compounds (0.6 μL, 10 mM) were added to the assay buffer. PLpro enzyme solution (10 nM final concentration) was prepared in the presence of each of the four lead inhibitors at a concentration equal to its IC_{50} value. PLpro in the absence of any inhibitors was also prepared as controls. Enzyme–lead inhibitor mixture solution (10 μL) was then added to the plates containing the Zenobia compounds, and the plates were incubated for an additional 5–10 min. The reaction was initiated by adding substrate (7.5 μL, 75 μM final concentration), and fluorescence intensity was continuously monitored with a POLARstar OPTIMA microplate reader (BMG LABTECH) for 10 min. All compounds were tested in duplicate, and each plate contained a total of 16 positive and 16 negative controls.

IC_{50} value determinations: The IC_{50} values of each fragment compound that showed synergistic inhibitory activity were determined. The hit compounds were prepared at various concentrations (0–1000 μM). The IC_{50} values of the four lead inhibitors were measured in the same concentrations of enzyme and substrate as the initial screening with a series of the lead compound concentrations (0–20 μM) in the absence and presence of 200 μM hit compounds. The reaction was initiated by adding fluorogenic substrate, and its activity was continuously monitored. The IC_{50} values were calculated by fitting to the three-parameter Hill equation [Eq. (1)] with OriginPro 8.5 (OriginLab, Inc.):

$$y = V_{max}\left(\frac{x^n}{IC_{50}^n + x^n}\right) \quad (1)$$

for which y is percent inhibition, x is inhibitor concentration, n is the slope of the concentration–response curve (Hill slope), and V_{max} is maximal inhibition from three independent assays.

Reversibility of fragment inhibition: The reversibility of the hit fragment compounds was determined by the dilution method.[22] PLpro enzyme was prepared as a 400 nM solution (20× assay concentration) and was incubated with screened compounds at 20× each IC_{50} concentration for 30 min at room temperature in assay buffer containing 50 mM HEPES pH 7.5, 2 mM GSH, 0.01% Triton, 0.1 mg mL^{-1} BSA, and 1% DMSO in a final volume of 200 μL. PLpro with the same amount of DMSO in place of fragment compounds was also prepared in the same way as a control. The activity of PLpro was measured in the same way as IC_{50} measurements. The enzyme–inhibitor solution was then diluted 20- and 40-fold and incubated for 30 min before measurement of percent recovery of enzyme activity. All reversibility assays were done in triplicate.

Determination of dissociation equilibrium constant (K_D) by SPR: Untagged native PLpro enzyme was prepared in PBS (10 mM phosphate pH 7.4, 2.7 mM KCl, 137 mM NaCl) and immobilized on a CM5 sensor chip using standard amine coupling at 20 °C with running buffer HBS-P (10 mM HEPES, 150 mM NaCl, 0.05% surfactant P-20, pH 7.4) from GE healthcare using a Biacore T100 instrument. Flow channels 1 and 3 were activated by a mixture of 1-ethyl-3-(3-dimethylaminopropyl)carbodiimide hydrochloride (EDC)/*N*-hydroxy succinimide (NHS), and the activated surface was blocked by ethanolamine (pH 8.5) as controls. PLpro enzyme was diluted in 10 mM sodium acetate (pH 5.0) and immobilized to flow channels 2 and 4 after sensor surface activation with EDC/NHS with a 7 min injection followed by ethanolamine blocking on unoccupied surface area. PLpro immobilization levels of flow channels 2 and 4 were ~12500 and ~8500 RU, respectively. The four previously discovered inhibitors and seven identified Zenobia fragment compounds were prepared as 10 mM (inhibitors **1**–**4**) or 200 mM (fragments) DMSO stocks. Compound solutions with a series of increasing concentrations (0–20 μM for inhibitors, 0–800 μM for fragments at 1.5-fold dilution) were applied to all four channels at a flow rate of 10 μL min^{-1}. Sensorgrams were analyzed using Biaevaluation software 2.0.3, and response unit difference (ΔRU) values at each concentration were measured during the binding equilibration phase. SigmaPlot 11.0 was used to fit the data to a single rectangular hyperbolic curve to determine K_D values. The hyperbola function, $y = y_{max} \cdot x/(K_D + x)$, was used to plot response units and corresponding concentration, where y is the response, y_{max} is the maximum response, and x is the compound concentration.

Mechanism of inhibition: PLpro activity was monitored in the same way as the primary screening with varying concentrations of both inhibitor compounds and substrate (0–300 μM). The concentration of compounds was varied from 0 to at least 10× the IC_{50} value of each fragment. The data were fit to the following equations using SigmaPlot Enzyme Kinetics Module 1.3 to determine the best fit inhibition mechanism and kinetic parameters for each compound:

$$\text{Competitive}: \quad \nu = \frac{V_{max}}{\left(1 + \frac{K_m}{[S]}\right) + \left(1 + \frac{I}{[K_i]}\right)} \quad (2)$$

$$\text{Noncompetitive}: \quad \nu = \frac{V_{max}}{\left(1 + \frac{I}{[K_i]}\right) + \left(1 + \frac{K_m}{[S]}\right)} \quad (3)$$

$$\text{Uncompetitive}: \quad \nu = \frac{V_{max}}{1 + \frac{I}{[K_i]} + \frac{K_m}{[S]}} \quad (4)$$

$$\text{Mixed-type}: \quad \nu = \frac{V_{max}}{\left(\frac{K_m}{[S]}\right)\left(1+\frac{[I]}{K_i}\right)+\left(1+\frac{[I]}{\alpha K_i}\right)} \tag{5}$$

for which v is the reaction rate, V_{max} is the maximum rate of the reaction, K_m is the Michaelis–Menten constant for substrate, [S] is the substrate concentration, [I] is the inhibitor concentration, K_i is the dissociation constant of the inhibitor I from the free enzyme, and αK_i is the dissociation constant for the inhibitor I from the ES complex.

Computational studies

Fragment binding site analysis: All MD simulations were performed using the AMBER suite of programs (AMBER 11).[23] The two known co-crystal structures (inhibitor-bound, PDB IDs: 3E9S and 3MJ5) were obtained from the RCSB Protein Data Bank. Multimer protein complexes were reduced to the functional monomer form for simulations. The bound inhibitor and zinc ions were retained in the systems; all other ions and crystal waters were removed. The ligand parameters were generated using the Antechamber software in AmberTools v1.5 and the General Amber Force Field (GAFF) with am1bcc charges.[24] Leap was used to neutralize the systems by adding sodium ions, and each system was solvated using 8 Å TIP3P water in a rectangular box. The systems were prepared using the ff99SB Force Field.[25] Minimization using SANDER was carried out in two steps: first, only the water molecules were minimized for 5000 steps while keeping the protein fixed; second, the entire system was minimized for an additional 10000 steps. Periodic boundary conditions were applied with 8 Å of nonbonded cutoff. The systems were heated from 0 to 300 K using the NVT ensemble in 50 ps with positional restraint on the protein. Following this, the systems were equilibrated for 100 ps using the NPT ensemble without restraint. The production phase of the simulation was performed using the NPT ensemble without positional restraint for 50 ns. Post-analysis was performed using the ptraj module from AmberTools v1.5 to compute the average structures at every 1 ns and write out the PDB file for the averaged coordinates. A total of 50 snapshots were extracted using this method.

The PDB files generated above were uploaded to the FTMAP server (http://ftmap.bu.edu/). The FTMAP server removes any waters, ions, and bound ligands and only retains the protein structure. Sixteen different probes were used: ethanol, isopropanol, isobutanol, acetone, acetaldehyde, dimethyl ether, cyclohexane, ethane, acetonitrile, urea, methylamine, phenol, benzaldehyde, benzene, acetamide, and *N*,*N*-dimethylformamide. The output results generated by FTMAP were in the form of PDB files with consensus clusters of the different probes mapped to the surface of the PLpro structure. Cluster sites identified by FTMAP were required to be conserved among all molecular probes for selection and further study, described below. Two such sites were identified (see Discussion above). One additional candidate binding site, site 3, was identified using coarse docking studies, described below.

Binding affinity predictions: To further investigate potential binding sites, fragments were docked to the enzyme using Glide-XP (extra precision) and the Induced Fit Docking (IFD) protocol of Schrödinger, using default settings.[26] The structures of PLpro bound with GRL-0617S (PDB ID: 3E9S) and GRL-0667S (PDB ID: 3MJ5) were obtained from the RCSB Protein Data Bank. Prior to molecular docking, structures of protein targets were prepared using the Protein Preparation Wizard in the Schrödinger software package (Suite 2012). All water molecules in the crystal structures were removed, and crystal multimers were reduced to the monomer. Residues located within 5 Å of the bound inhibitors were refined by the Prime algorithm. Two distinct docking runs were performed using this strategy. The first docking run was blind docking (coarse docking), with the docking area defined to be within 10 Å of the lead inhibitors. Candidate site 3 was identified during these studies as a high-scoring binding site for multiple fragments. The subsequent docking runs were defined by the location of the candidate sites identified by the structural and computational analyses, described above. Binding site 1 (the catalytic site) was defined by selecting residues H273, C112, and D287; binding site 2 was defined by selecting residues R167, E168, M209, D303, and T302; and binding site 3 was defined by selecting residues N157, K158, D165, and E168. Binding hot spot 2 was not studied for the reasons described above. In each case, the docking area was defined to be a 10 Å box centered on the selected residues. Fragments of the Zenobia library were prepared in multiple tautomer and protonation states at pH 7.4 by using LigPrep (Schrödinger).[27] All eight active fragments were docked in the coarse docking studies; only fragment **F8** was docked in the subsequent candidate site docking studies. All docking poses were ranked by Glide XP score.[28] In the second docking run, three conformations (poses) each of **F8** at each binding site (sites 1, 2, and 4) produced by IFD were selected as the starting conformations for the MD simulations and subsequent MM/PBSA calculation, described below. The binding poses selected included the top score pose and two other poses which possessed the greatest difference (by calculated RMSD).

MD simulations and subsequent MM/PBSA calculations used to predict binding affinities were performed using the AMBER suite of programs (AMBER 11).[23] Preparation of the MD simulations, including parameterization of the fragment (**F8**) and inhibitors, and preparation and equilibration of the system, were performed exactly as described above for binding site analyses. The production phase of the simulation was performed using the NPT ensemble without positional restraints for 20 ns. The python script, MMPBSA.py, included in AMBER 11, was used to perform the MM/PBSA calculations.[29] The first 100 frames from the last 2 ns (equilibrated) of the simulation trajectory file were used for the MM/PBSA calculations. The ionic strength was set to 0.1 M, and the internal dielectric constant was set as 1.0 (default). All other options were set to default settings. The values for the free energy of binding of each inhibitor, combined with the three different fragment poses, were calculated according to Equation (6):

$$\Delta G_{bind} = G_{complex} - G_{receptor} - G_{ligand} \tag{6}$$

in which $G_{complex}$ is the calculated Gibbs free energy of the inhibitor–fragment–enzyme complex, $G_{receptor}$ is the Gibbs free energy for the fragment–enzyme complex, and G_{ligand} is the Gibbs free energy calculated for the inhibitor compounds. The free energy values for each of these terms were estimated as the sum of the four terms:

$$G = E_{MM} + G_{psolv} + G_{npsolv} - TS_{nmode} \tag{7}$$

in which E_{MM} is the molecular mechanics energy of the molecule expressed as the sum of the internal energy of the molecule plus the electrostatics and van der Waals interactions; G_{psolv} is the polar contribution to the solvation energy of the molecule; G_{npsolv} is the nonpolar solvation energy; T is the absolute temperature; and S is the vibrational, rotational, and translational entropy of the molecule estimated by normal mode analysis, using five regularly spaced snapshots from the first 100 frames in the last 2 ns of the

MD simulations. Ionic strength in normal mode calculations was set as 0.1 M.

Fragment merging and docking: A fragment merging strategy was employed based on the binding conformations observed from MM/PBSA studies (Figure 6). The proposed compounds were designed by merging the structures of lead inhibitors with fragment **F8**. The nitroaromatic ring was deleted, and the remaining piperazine ring was attached to several different sites on the lead inhibitors using a variety of different linking groups. With the goal of retaining the lead binding position of the inhibitor scaffold after docking the merged hybrids, we investigated several alternative linking strategies, including linking to the naphthalene ring, the chiral methyl group, and the *p*-toluidine (scaffold **A**) or methylenedioxybenzene (scaffold **B**) by alkyl groups, ester groups, and amide groups. The binding conformations of the virtually generated hybrid collection were predicted using Glide docking with SP scoring. The structures of PLpro bound with GRL-0617S (PDB ID: 3E9S) and GRL-0667S (PDB ID: 3MJ5) were used in these docking studies and prepared using the Schrödinger protein preparation software as described above. The docking site was defined as a 10 Å box centered on the original binding site of the lead inhibitors. The hybrid compound library was prepared as described above for fragment and inhibitor docking. Proposed compounds discussed above were selected by score and visual comparison with the crystallographic position of the lead inhibitor and the predicted binding conformation of the fragment.

Supporting Information

The replicate plot, ligand efficiency indices, binding free energy calculations, and NMR spectra of fragment hit compounds are included in the Supporting Information.

Acknowledgements

This work was supported by US National Institutes of Health (NIH) Grant R56 AI089535. This work used the Extreme Science and Engineering Discovery Environment (XSEDE), which is supported by National Science Foundation grant number OCI-1053575. K.E.H. was supported during a portion of this work by US National Institute of Dental and Craniofacial Research (NIDCR) 5T32-DE018381, University of Illinois at Chicago College of Dentistry, MOST program. Molecular graphics images were produced using the UCSF Chimera package from the Resource for Biocomputing, Visualization, and Informatics at the University of California, San Francisco (supported by US NIH grant P41 RR001081). We thank ChemAxon Ltd. for an academic research license of their cheminformatics suite including JChem and JChem for Excel for data analysis. H.L. performed all experiments with assistance of L.T., J.L.G., and K.P. S.C. and K.E.H. performed computational studies. A.K.G. synthesized current lead compounds. H.L., S.C., K.E.H., and M.E.J. designed the experiments and wrote the manuscript.

Keywords: fragments · human SARS coronavirus · inhibitors · papain-like protease · small molecules

[1] a) C. Drosten, S. Gunther, W. Preiser, S. van der Werf, H. R. Brodt, S. Becker, H. Rabenau, M. Panning, L. Kolesnikova, R. A. Fouchier, A. Berger, A. M. Burguiere, J. Cinatl, M. Eickmann, N. Escriou, K. Grywna, S. Kramme, J. C. Manuguerra, S. Muller, V. Rickerts, M. Sturmer, S. Vieth, H. D. Klenk, A. D. Osterhaus, H. Schmitz, H. W. Doerr, *N. Engl. J. Med.* **2003**, *348*, 1967 – 1976; b) T. G. Ksiazek, D. Erdman, C. S. Goldsmith, S. R. Zaki, T. Peret, S. Emery, S. Tong, C. Urbani, J. A. Comer, W. Lim, P. E. Rollin, S. F. Dowell, A. E. Ling, C. D. Humphrey, W. J. Shieh, J. Guarner, C. D. Paddock, P. Rota, B. Fields, J. DeRisi, J. Y. Yang, N. Cox, J. M. Hughes, J. W. LeDuc, W. J. Bellini, L. J. Anderson, *N. Engl. J. Med.* **2003**, *348*, 1953 – 1966; c) J. S. Peiris, S. T. Lai, L. L. Poon, Y. Guan, L. Y. Yam, W. Lim, J. Nicholls, W. K. Yee, W. W. Yan, M. T. Cheung, V. C. Cheng, K. H. Chan, D. N. Tsang, R. W. Yung, T. K. Ng, K. Y. Yuen, *Lancet* **2003**, *361*, 1319 – 1325.

[2] a) N. Barretto, D. Jukneliene, K. Ratia, Z. Chen, A. D. Mesecar, S. C. Baker, *J. Virol.* **2005**, *79*, 15189 – 15198; b) S. K. Lau, P. C. Woo, K. S. Li, Y. Huang, H. W. Tsoi, B. H. Wong, S. S. Wong, S. Y. Leung, K. H. Chan, K. Y. Yuen, *Proc. Natl. Acad. Sci. USA* **2005**, *102*, 14040 – 14045.

[3] a) P. C. Woo, S. K. Lau, C. M. Chu, K. H. Chan, H. W. Tsoi, Y. Huang, B. H. Wong, R. W. Poon, J. J. Cai, W. K. Luk, L. L. Poon, S. S. Wong, Y. Guan, J. S. Peiris, K. Y. Yuen, *J. Virol.* **2005**, *79*, 884 – 895; b) K. Pyrc, B. Berkhout, L. van der Hoek, *J. Virol.* **2007**, *81*, 3051 – 3057.

[4] a) R. A. Fouchier, N. G. Hartwig, T. M. Bestebroer, B. Niemeyer, J. C. de Jong, J. H. Simon, A. D. Osterhaus, *Proc. Natl. Acad. Sci. USA* **2004**, *101*, 6212 – 6216; b) L. van der Hoek, K. Pyrc, M. F. Jebbink, W. Vermeulen-Oost, R. J. Berkhout, K. C. Wolthers, P. M. Wertheim-van Dillen, J. Kaandorp, J. Spaargaren, B. Berkhout, *Nat. Med.* **2004**, *10*, 368 – 373.

[5] a) A. M. Zaki, S. van Boheemen, T. M. Bestebroer, A. D. Osterhaus, R. A. Fouchier, *N. Engl. J. Med.* **2012**, *367*, 1814 – 1820; b) A. Bermingham, M. A. Chand, C. S. Brown, E. Aarons, C. Tong, C. Langrish, K. Hoschler, K. Brown, M. Galiano, R. Myers, R. G. Pebody, H. K. Green, N. L. Boddington, R. Gopal, N. Price, W. Newsholme, C. Drosten, R. A. Fouchier, M. Zambon, *Euro Surveillance* **2012**, *17*, 20290.

[6] a) B. C. Fielding, *Future Microbiol.* **2011**, *6*, 153 – 159; b) L. J. Cui, C. Zhang, T. Zhang, R. J. Lu, Z. D. Xie, L. L. Zhang, C. Y. Liu, W. M. Zhou, L. Ruan, X. J. Ma, W. J. Tan, *Adv. Virol.* **2011**, 129134.

[7] Novel coronavirus infection update: February 11, 2013, World Health Organization Global Alert and Response, http://www.who.int/csr/en/.

[8] S. van Boheemen, M. de Graaf, C. Lauber, T. M. Bestebroer, V. S. Raj, A. M. Zaki, A. D. Osterhaus, B. L. Haagmans, A. E. Gorbalenya, E. J. Snijder, R. A. M. Fouchier, *mBio* **2012**, *3*, e00473-12.

[9] a) H. Yang, M. Bartlam, Z. Rao, *Curr. Pharm. Des.* **2006**, *12*, 4573 – 4590; b) B. H. Harcourt, D. Jukneliene, A. Kanjanahaluethai, J. Bechill, K. M. Severson, C. M. Smith, P. A. Rota, S. C. Baker, *J. Virol.* **2004**, *78*, 13600 – 13612.

[10] a) A. K. Ghosh, G. Gong, V. Grum-Tokars, D. C. Mulhearn, S. C. Baker, M. Coughlin, B. S. Prabhakar, K. Sleeman, M. E. Johnson, A. D. Mesecar, *Bioorg. Med. Chem. Lett.* **2008**, *18*, 5684 – 5688; b) A. K. Ghosh, K. Xi, V. Grum-Tokars, X. Xu, K. Ratia, W. Fu, K. V. Houser, S. C. Baker, M. E. Johnson, A. D. Mesecar, *Bioorg. Med. Chem. Lett.* **2007**, *17*, 5876 – 5880; c) A. K. Ghosh, K. Xi, K. Ratia, B. D. Santarsiero, W. Fu, B. H. Harcourt, P. A. Rota, S. C. Baker, M. E. Johnson, A. D. Mesecar, *J. Med. Chem.* **2005**, *48*, 6767 – 6771; d) R. P. Jain, H. I. Pettersson, J. Zhang, K. D. Aull, P. D. Fortin, C. Huitema, L. D. Eltis, J. C. Parrish, M. N. James, D. S. Wishart, J. C. Vederas, *J. Med. Chem.* **2004**, *47*, 6113 – 6116; e) R. P. Jain, J. C. Vederas, *Bioorg. Med. Chem. Lett.* **2004**, *14*, 3655 – 3658; f) J. J. Shie, J. M. Fang, C. J. Kuo, T. H. Kuo, P. H. Liang, H. J. Huang, W. B. Yang, C. H. Lin, J. L. Chen, Y. T. Wu, C. H. Wong, *J. Med. Chem.* **2005**, *48*, 4469 – 4473.

[11] a) A. K. Ghosh, J. Takayama, Y. Aubin, K. Ratia, R. Chaudhuri, Y. Baez, K. Sleeman, M. Coughlin, D. Nichols, D. C. Mulhearn, B. S. Prabhakar, S. C. Baker, M. E. Johnson, A. D. Mesecar, *J. Med. Chem.* **2009**, *52*, 5228 – 5240; b) A. K. Ghosh, J. Takayama, K. V. Rao, K. Ratia, R. Chaudhuri, D. C. Mulhearn, H. Lee, D. B. Nichols, S. Baliji, S. C. Baker, M. E. Johnson, A. D. Mesecar, *J. Med. Chem.* **2010**, *53*, 4968 – 4979.

[12] C. Y. Chou, C. H. Chien, Y. S. Han, M. T. Prebanda, H. P. Hsieh, B. Turk, G. G. Chang, X. Chen, *Biochem. Pharmacol.* **2008**, *75*, 1601 – 1609.

[13] J. Y. Park, H. J. Jeong, J. H. Kim, Y. M. Kim, S. J. Park, D. Kim, K. H. Park, W. S. Lee, Y. B. Ryu, *Biol. Pharm. Bull.* **2012**, *35*, 2036 – 2042.

[14] K. Ratia, K. S. Saikatendu, B. D. Santarsiero, N. Barretto, S. C. Baker, R. C. Stevens, A. D. Mesecar, *Proc. Natl. Acad. Sci. USA* **2006**, *103*, 5717 – 5722.

[15] K. Ratia, S. Pegan, J. Takayama, K. Sleeman, M. Coughlin, S. Baliji, R. Chaudhuri, W. Fu, B. S. Prabhakar, M. E. Johnson, S. C. Baker, A. K.

Ghosh, A. D. Mesecar, *Proc. Natl. Acad. Sci. USA* **2008**, *105*, 16119 – 16124.
[16] a) C. W. Murray, M. L. Verdonk, D. C. Rees, *Trends Pharmacol. Sci.* **2012**, *33*, 224 – 232; b) C. W. Murray, T. L. Blundell, *Curr. Opin. Struct. Biol.* **2010**, *20*, 497 – 507; c) S. B. Shuker, P. J. Hajduk, R. P. Meadows, S. W. Fesik, *Science* **1996**, *274*, 1531 – 1534; d) Y. S. Wang, C. Strickland, J. H. Voigt, M. E. Kennedy, B. M. Beyer, M. M. Senior, E. M. Smith, T. L. Nechuta, V. S. Madison, M. Czarniecki, B. A. McKittrick, A. W. Stamford, E. M. Parker, J. C. Hunter, W. J. Greenlee, D. F. Wyss, *J. Med. Chem.* **2010**, *53*, 942 – 950; e) R. A. Ward, C. Brassington, A. L. Breeze, A. Caputo, S. Critchlow, G. Davies, L. Goodwin, G. Hassall, R. Greenwood, G. A. Holdgate, M. Mrosek, R. A. Norman, S. Pearson, J. Tart, J. A. Tucker, M. Vogtherr, D. Whittaker, J. Wingfield, J. Winter, K. Hudson, *J. Med. Chem.* **2012**, *55*, 3285 – 3306.
[17] C. Abad-Zapatero, J. T. Metz, *Drug Discovery Today* **2005**, *10*, 464 – 469.
[18] C. Abad-Zapatero, O. Perisic, J. Wass, A. P. Bento, J. Overington, B. Al-Lazikani, M. E. Johnson, *Drug Discovery Today* **2010**, *15*, 804 – 811.
[19] a) W. J. Egan, K. M. Merz, Jr., J. J. Baldwin, *J. Med. Chem.* **2000**, *43*, 3867 – 3877; b) K. Palm, P. Stenberg, K. Luthman, P. Artursson, *Pharm. Res.* **1997**, *14*, 568 – 571; c) P. Ertl, B. Rohde, P. Selzer, *J. Med. Chem.* **2000**, *43*, 3714 – 3717.
[20] K. P. Burnham, D. R. Anderson, *Model Selection and Inference*, Springer, New York, **1998**.
[21] C. H. Ngan, T. Bohnuud, S. E. Mottarella, D. Beglov, E. A. Villar, D. R. Hall, D. Kozakov, S. Vajda, *Nucleic Acids Res.* **2012**, *40*, W271 – 275.
[22] "Lead Optimization and SAR for Reversible Inhibitors": R. A. Copeland in *Evaluation of Enzyme Inhibitors in Drug Discovery*, Wiley, Hoboken, **2005**.
[23] D. A. Case, T. A. Darden, T. E. Cheatham III, C. L. Simmerling, J. Wang, R. E. Duke, R. Luo, R. C. Walker, W. Zhang, K. M. Merz, B. P. Roberts, B. Wang, S. Hayik, A. Roitberg, G. Seabra, I. Kolossvary, K. F. Wong, F. Paesani, J. Vanicek, X. Wu, S. R. Brozell, T. Steinbrecher, H. Gohlke, Q. Cai, X. Ye, J. Wang, M.-J. Hsieh, G. Cui, D. R. Roe, D. H. Mathews, M. G. Seetin, C. Sagui, V. Babin, T. Luchko, S. Gusarov, A. Kovalenko, P. A. Kollman, AMBER 11, University of California, San Francisco, **2010**.
[24] a) J. Wang, R. M. Wolf, J. W. Caldwell, P. A. Kollman, D. A. Case, *J. Comput. Chem.* **2004**, *25*, 1157 – 1174; b) J. Wang, W. Wang, P. A. Kollman, D. A. Case, *J. Mol. Graphics Modell.* **2006**, *25*, 247 – 260; c) A. Jakalian, D. B. Jack, C. I. Bayly, *J. Comput. Chem.* **2002**, *23*, 1623 – 1641.
[25] V. Hornak, R. Abel, A. Okur, B. Strockbine, A. Roitberg, C. Simmerling, *Proteins* **2006**, *65*, 712 – 725.
[26] Schrödinger Suite 2012 Induced-Fit Docking Protocol; Glide version 5.8, Prime version 3.1, Schrödinger LLC, New York, NY (USA), **2012**.
[27] Suite 2012: LigPrep version 2.5, Schrödinger LLC, New York, NY (USA), **2012**.
[28] R. A. Friesner, R. B. Murphy, M. P. Repasky, L. L. Frye, J. R. Greenwood, T. A. Halgren, P. C. Sanschagrin, D. T. Mainz, *J. Med. Chem.* **2006**, *49*, 6177 – 6196.
[29] B. R. Miller, D. T. McGee, J. M. Swails, N. Homeyer, H. Gohlke, A. E. Roitberg, *J. Chem. Theory Comput.* **2012**, *8*, 3314 – 3321.

Received: March 25, 2013
Revised: May 29, 2013
Published online on June 20, 2013